MAGRAC—A RAILGUN SIMULATION PROGRAM

F. J. Deadrick
R. S. Hawke
J. K. Scudder

MASTER

October 24, 1980

Lawrence Livermore Laboratory

MAGRAC--A RAILGUN SIMULATION PROGRAM[*]
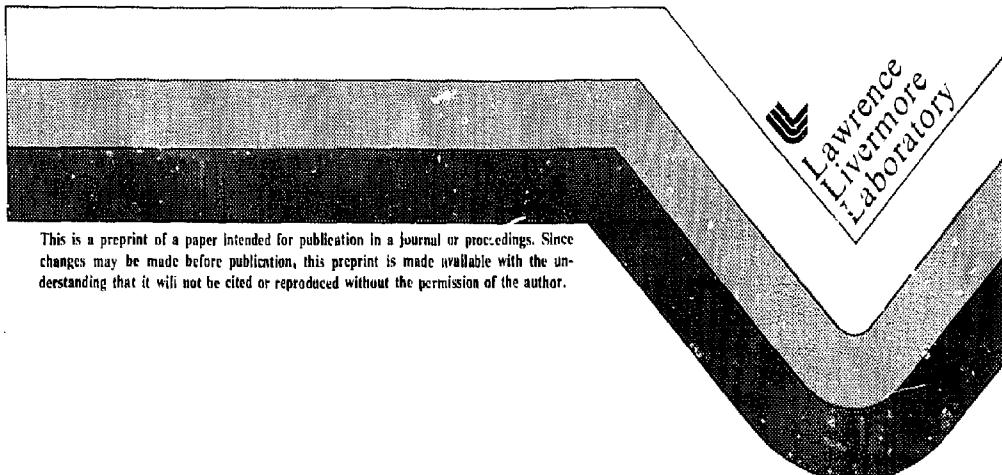
F. J. Deadrick
R. S. Hawke
J. K. Scudder[†]
Lawrence Livermore National Laboratory
Livermore, Calif.

ABSTRACT

We have developed and validated a computer simulation code at the

Lawrence Livermore National Laboratory (LLNL) to predict the performance of a

railgun electromagnetic accelerator. The code, called MAGRAC (MAGnetic

Railgun ACcelerator), models the performance of a railgun driven by a magnetic

flux compression current generator (MFCG). The MAGRAC code employs a

time-step solution of the nonlinear time-varying element railgun circuit to

determine rail currents. From the rail currents, the projectile acceleration,

velocity, and position is found. We have validated the MAGRAC code through a

series of eight railgun tests conducted jointly with the Los Alamos Scientific

National Laboratory. This paper describes the formulation of the MAGRAC

railgun model and compares the predicted current waveforms with those obtained

from full-scale experiments.

INTRODUCTION

MAGRAC (MAGnetic Railgun ACcelerator) is a computer code designed to model an electromagnetic railgun projectile launcher and power source. The MAGRAC code uses both electrical and mechanical parameters of the railgun, projectile, and primary energy source to compute the resulting currents and accelerating forces on the projectile as a function of time. The code employs an implicit finite-difference solution technique which allows the inclusion of time-varying nonlinear elements in the railgun model.

In this paper we describe the model elements used in the MAGRAC code and compare some computed results with railgun test data. Three series of tests have been conducted in collaboration with the Los Alamos National Scientific Laboratory (LANSL) to test the performance of railgun accelerators. These tests included both 0.9-m and 1.8-m long railguns with square bores of 12.7 mm that were used to launch 3.1-gram polycarbonate projectiles. Also a short, 0.3-m long, 50-mm square bore gun was used to launch a 165-gram projectile. In each of these tests, a magnetic flux compression generator[1] (MFCG) was used as the primary energy source to power the railgun. The MAGRAC model includes both the railgun and a variety of power sources including the MFCG.

We first provide brief details of the railgun and the MFCG. We then describe the computer solution technique and conclude with representative comparisons between computer prediction and experiment.

MAGRAC MODELS

Figure 1 shows a simplified, schematic illustration of a railgun. A railgun is essentially a linear dc motor consisting of a pair of rigid parallel bars (rails) that carry current to and from a small interconnecting moveable conductor. The conducting link functions as an armature, while the parallel rails serve as a single-turn field winding. The Lorentz force resulting from the armature current interacting with the magnetic field generated by the rail current accelerates the armature and the projectile.

While railguns may be driven by a number of primary energy sources such as capacitor banks and homopolar generators, we discuss only the MFCG in this report.

The MFCG-railgun system used by the joint LANSL/LLNL team is shown in Fig. 2. The capacitor bank provides the initial energy to the circuit, and the MFCG extends the duration of the current pulse delivered to the railgun. When the switch is closed, the capacitor bank generates a current in the MFCG which acts as a temporary storage inductor. As the current approaches near maximum, the explosive is initiated by a single detonator. The explosive drives the top conductor of the MFCG into the bottom conductor, isolates the capactor bank source at point A, forms a closed MFCG-railgun circuit, and continues to progressively implode the MFCG. The resulting decrease in inductance tends to sustain the current, while energy is consumed by the railgun and losses.

RAILGUN MODEL

The railgun portion of the model is basically very simple in form. Two
copper rails provide the current path for the accelerator. A small fuse is
placed at the breech end of the gun section directly behind the projectile.
The fuse serves two purposes, the first being to provide a current path for
the initial MFCG current charge, and secondly to generate a plasma arc between
the rails to act as a moveable conducting armature.

An electrical equivalent circuit of the railgun section is shown in
Fig. 3. $R(x,t,I)$ is the rail resistance term which changes as a function of
the plasma armature position x, time t, and rail current I. Rail heating
occurs as a result of the resistive energy loss which increases the
temperature and resistivity of the rails. The effective rail resistivity ρ
(see appendix A) is represented by the relation

$$\rho = \rho_0 + \rho_T\left(\frac{I}{p}\right)$$ (1)

where ρ_0 is the initial resistivity of the copper rails, ρ_T is a
temperature-dependent restivity coefficient, and p is the width of the rails.
Time-dependent diffusion of a constant current into the rails in combination
with a freely accelerating projectile leads to an effective rail resistance
gradient (effective resistance per unit rail length), R_1, (see appendix B)

$$R_1 = \frac{8}{3p}\ (\pi\mu\rho/2t)^{1/2}$$ (2)

where μ is the permeability of the rail material, and t is the length of
time that the current has been flowing.

The inductance L of the rail pair enters into both the electrical circuit equations and the equations of motion. Electrically, as the armature moves down the bore of the railgun, both the gun resistance and inductance increase, as more of the rail pair is included in the circuit. The resulting inductive voltage V_L is given by:

$$V_L = \frac{d(LI)}{dt} = L \frac{dI}{dt} + I \frac{dL}{dt} \quad , \tag{3}$$

where

$$L = L_1 x \quad , \tag{4}$$

$$\frac{dL}{dt} = L_1 \frac{dx}{dt} = L_1 v \tag{5'}$$

and L_1 is the inductance gradient (inductance per unit length of the rail pair), and v is the armature velocity.

A third term, the plasma arc voltage drop V_{Arc}, is also included in the model, as shown in Fig. 3.

When the fuse vaporizes and establishes the initial plasma arc, the plasma acts as a moveable conductor which "pushes" on the projectile and accelerates the mass down the barrel of the gun. The Lorentz force F_p on the projectile is given by:

$$F_p = \frac{L_1 I^2}{2} \tag{6}$$

and the projectile acceleration, a, is:

$$a \approx \frac{L_1 I^2}{2m} \tag{7}$$

where m is the mass of the projectile. Projectile velocity and position are then obtained from the first and second integrals of the projectile acceleration, respectively.

MFCG MODEL

The model for the flux compression generator is similar in form to that of the railgun section in that the MFCG is primarily a time-varying inductor and resistor. Figure 4 illustrates the electrical equivalent circuit model for the MFCG and the capacitor bank used to supply the initial generator current.

In the initial state, the switch S_2 is open, and S_1 is closed at $t = 0$ to connect the capacitor bank to the compression generator. The RLC elements of the capacitor bank, MFCG, and railgun fuse form a damped resonant circuit which has a sinusoidal current buildup in the MFCG. One typically closes the switch S_2 near the peak current of the first-quarter cycle.

The MAGRAC model includes both the capacitor bank charge-up cycle and the compression of the MFCG which is modelled as a short which moves down the length of the MFCG at the explosive detonation velocity. The MFCG resistance term, R_F, is modeled as a function of the position of the short, the time, and the current.

The resistance is calculated from the MFCG conductor resistivity, ρ_F, where,

$$\rho_F = \rho_{F0} + \rho_{FT}\left(\frac{I_F}{\rho_F}\right) \tag{8}$$

and, ρ_{F0} is the initial resistivity of the MFCG conductors. I_F is the MFCG current and ρ_F is the width of the flux compression conductors. The effective resistance gradient R_{1F} of the MFCG (see appendix B) is then evaluated as a function of time and current,

$$R_{1F} = \frac{1}{\rho_F}(\pi\mu\rho_F/2t)^{1/2} \tag{9}$$

The equivalent MFCG resistance term for both conductors in the equivalent circuit is

$$R_F = 2R_{1F}(z_0 - z) \tag{10}$$

where z_0 is the initial length of the generator, and z is the length of MFCG which has been imploded.

The terms for the MFCG inductance are somewhat more complex. As the HE burns, the overall length of the MFCG circuit diminishes and thereby the resistance and inductance in the circuit become smaller. The high currents on the other hand force the generator conductors apart. The LANSL design uses a steel bar to inertially confine the generator during operation; however, at high current levels the rails of the MFCG move apart resulting in an increase in the inductance. Appendix C describes the technique used to calculate the time-varying inductance gradient, L_{1F}, from which the MFCG inductance, L_F, is calculated, where

$$L_F = L_{1F}(z_0 - z) \quad . \tag{11}$$

COMPUTER SOLUTION

When the railgun section and the MFCG section are combined as shown in Fig. 5, circuit equations can be written for the various portions of circuit operation, i.e., after S_1 is closed and before S_2 is closed, etc. The capacitor bank charge voltage is used as an initial condition for the start of the simulation. When S_1 is closed, the bank is connected to the MFCG and the railgun fuse shunt. The model integrates the energy dissipated in the fuse to determine the time of vaporization. We evaluate the current by using Kirchoff's law to calculate the derivative of the current circulating in each electrical loop and then incrementally change the current with each iteration. Once each iteration of $I(t)$ is found, we then use this value to compute a new set of values for dI/dt, etc. The MAGRAC code keeps account of the various regions of operation to select the proper expressions for the computation of the circuit currents.

As the MAGRAC code computes the MFCG and railgun currents at each time step, the railgun current is used to calculate the Lorentz accelerating force on the projectile. The projectile acceleration is integrated once to compute the projectile velocity and twice to determine the projectile position. The updated current, velocity, and position values in turn feed back into the evaluation of parameters used to compute the new value of dI/dt.

To illustrate the results obtained from the MAGRAC code, representative computations and experimental measurements are shown in the next section.

NUMERICAL RESULTS

The MACRAC code has been used to model several of the joint LLNL/LANSL railgun experiments conducted at Los Alamos.[2] Table 1 summarizes these experiments. The diagnostics used in these tests included pulsed x rays to observe the projectile in flight; Rogowski coils to monitor the railgun-MFCG current; optical and inductive pickup probes to detect the plasma arc passage along the barrel of the railgun; and foil switches to detect the arrival times of the projectile. These diagnostics provided measured benchmarks with which to evaluate the numerical MACRAC model for several different railgun conditions.

75-kJ Short-Circuit Experiment

Shown first in Fig. 6 is the computed and measured current generated by a MFCG into a low-inductance short circuit. Using appropriate initial conditions and an inductance gradient for the MFCG of 0.46 μH/m, we found that the model provided good agreement with the experiment.

70-kJ/12.7-mm Bore Railgun Experiment

Figures 7a through 7c show the computed results for a railgun connected to the MFCG. This case, which corresponds to experiment 1A, is for a low-energy (70-kJ)/low-velocity (2.8-km/s) launch. In this experiment, we again obtained good agreement between computed and measured current and the

pulsed x-ray shadowgraph of the projectile in flight provided a benchmark for determining model accuracy as shown in Fig. 7c.

385-kJ/50-mm Bore Railgun Experiment

Good confirmation of the model has also been obtained for the large-bore 50mm-shot in which a 165-g projectile was launched from a 0.3-m long railgun. Figures 8a, b, and c show the measured and modeled current pulse, the predicted projectile position vs time, and the velocity vs position. Again, the computed and measured current record matched, and the shadowgraph record corresponded reasonably closely with the calculated position vs time. The slight shadowgraph-position mismatch results from a slightly higher computed velocity (Fig. 8c) accentuated by the long free-flight time.

395-kJ/12.7-mm Bore Railgun Experiment

As a final example, we include a comparison of the measured and modelled results for one of the high-energy (390 kJ)/high-velocity launches. Figures 9a, b, and c show the measured and modeled current pulse, the predicted projectile position vs time, and the velocity vs position for experiment 2C. Although a good match for the measured and calculated current vs time was obtained, particular sensitivity was observed in the terms containing the rail and flux generator widths, which enter into the calculations for the resistive terms. As discussed in a companion paper[5], shadowgraphs of the projectile after launch were not obtained in the high-energy/small-bore experiments; hence, the position vs time calculation cannot be verified as for the above experiments.

CONCLUSIONS

The MACRAC model has provided valuable insight and data which has directly benefited the design, operation, and diagnostics of MFCG-railgun systems used in the joint LANSL/LLNL research project. The agreement between experiment and calculation that was found for a wide variety of experiments has established the usefulness of the MAGRAC model. Further development of the MACRAC code and the performance of additional experiments will lead to an even firmer foundation for future predictions of railgun performance and their potential.

ACKNOWLEDGMENTS

REFERENCES

1. C. M. Fowler, D. R. Peterson, R. S. Caird, and D. J. Erickson, B. L.
    Freeman, and J. C. King, "Explosive Flux Compression Generators as Railgun
    Power Sources," Conference on Electromagnetic Guns and Launchers,
    Nov. 4-6, 1980, San Diego, CA. Published as Los Alamos National
    Scientific Laboratory, Los Alamos, NM, Report LA-UR-80-2542 (1980).

2. The MACRAC code has also been used[3] to model the Australian National
    University homopolar generator-inductor railgun system.[4]

3. R. S. Hawke and J. K. Scudder, "Magnetic Propulsion Railguns: Their Design
    and Capabilities," presented at the Second International Conference on
    Megagauss Magnetic Field Generation and Related Topics, May 29-June 1,
    1979, Washington, D.C., (to be published). Also published as Lawrence
    Livermore National Laboratory, Livermore, CA, Report UCRL-82677 (1979).

4. S. C. Rashleigh and R. A. Marshall, J. Appl. Phys. 49, 2540 (1978).

5. R. S. Hawke, A. L. Brooks, F. J. Deadrick, J. K. Scudder, C. M. Fowler,
    R. S. Caird, and D. R. Peterson, "Results of Railgun Experiments Powered
    by Magnetic Flux Compression Generators," Conference on Electromagnetic
    Guns and Launchers, Nov. 4-6, 1980, San Diego, CA. Published as Lawrence
    Livermore National Laboratory, Livermore. CA, Report UCRL-84875 (1980).

6. R. More, Lawrence Livermore National Laboratory, Livermore, CA, private communication (1979).

7. S. Seely, Introduction to Electromagnetic Fields (McGraw-Hill, inc. New York, 1958).

8. H. Knoepfel, Pulsed High Magnetic Fields (North-Holland Publishing Co., Amsterdam, 1970).

APPENDIX A. EQUIVALENT RESISTIVITY AS A

FUNCTION OF CURRENT CONCENTRATION

The effect of a temperature-dependent resistivity was determined by 1.) simultaneously solving the magnetic diffusion and heat transfer equations to determine the time-dependent current and temperature distributions in a semi-infinite conductor, 2) using the current distribution in combination with the temperature profile and resulting resistivity profile to calculate the effective resistance, and, 3) determine an equivalent resistivity which turned out to be a linear function of current concentration.

More[6] calculated the temperature rise and resistance of the rails as follows.

The current density j in the rails is given by

$$j = \frac{\partial H}{\partial y} \quad , \tag{A-1}$$

where H is the magnetic field, and y is the dimension normal to the rail surface. Because the dimensions of the rails are large compared to the current penetration depth, one-dimensional analysis is adequate.

The diffusion of H into the conductor is given by

$$\mu \frac{\partial H}{\partial t} = \frac{\partial}{\partial y} \left(\rho \frac{\partial H}{\partial y} \right) \quad , \tag{A-2}$$

and

$$DC_v \frac{\partial T}{\partial t} = \frac{\partial}{\partial y} \left(k \frac{\partial T}{\partial y} \right) + \rho \left(\frac{dH}{dy} \right)^2 \quad , \tag{A-3}$$

where μ is the permability, ρ is the resistivity, C_v is the specific

heat, k is the thermal conductivity, T is the temperature, and D is the mass

density of the rail material.

The electrical resistivity is assumed to be described by

$$\rho = \rho_0 + uT \quad , \tag{A-4}$$

where ρ_0 is the initial resistivity and u is the tempe. ture coefficient.

Equations (A-1) through (A-4) are solved as implicit finite-difference

equations, producing the temperature profile and resistance of the rails as

functions of time, rail dimensions, and current. Figures A-1, A-2 and A-3 are

typical sets of current, temperature, and resistivity profiles as functions of

time, respectively.

Next, the energy dissipated in the conductor was calculated by dividing

the semi-infinite conductor into thin regions, each with a resistance and

current element. The energy dissipated in each region was calculated and then

added together to find the total energy loss. The total energy loss and total

current lead to an equivalent resistance. The equivalent resistance was then

used to fi d an equivalent resistivity. The equivalent resistivity of several

current concentrations (current per unit rail width) were calculated in this

manner. It was found that the equivalent resistivity ρ_{eq} varied linearly

with the current concentration, leading to the simple relation

$$\rho_{eq} = \rho_0 + \rho_T \left(\frac{I}{p} \right), \tag{A-5}$$

where ρ_o is the initial normal resistivity, ρ_T is the current
concentration dependent component of resistivity, I is the total current, and
p is the rail width (see Fig. A-4). The form of Eq. (A-5) was used to
calculate the effective resistivity of the MFCG Eq. (8) and the railgun
Eq. (1) conductors.

APPENDIX B.   DERIVATION OF RESISTANCE OF

MFCG AND RAILGUN CONDUCTORS

MFCG

The current diffuses into the MFCG conductors uniformly along its length.
The effective resistance R per unit length l of each of the MFCG conductors
is given by

$$\frac{R}{l} \equiv R_{1F} = \frac{\mu_F}{p_F \delta} \tag{B-1}$$

where R_{1F} is the MFCG resistance gradient, ρ_F is the resistivity of the
MFCG conductors, p_F is the width of the conductors and δ is the skin depth
of the diffused current at time, t.

$$\delta = \left(\frac{2\rho_F t}{\pi\mu}\right)^{1/2} , \tag{B-2}$$

where μ is the permeability of the conductors.   Combining B-1 and B-2 we
have,

$$R_{1F} = \frac{\rho_F}{p_F\left(\frac{2\rho_F t}{\pi\mu}\right)^{1/2}} = \frac{1}{p_F}\left(\frac{\pi\mu\rho_F}{2t}\right)^{1/2} . \tag{B-3}$$

RAILGUN

Unlike the MFCG, the time that the current has had to diffuse into the rails is not uniform, but is a function of the time at each point along the rails that has passed since the projectile armature has passed that point. (See Fig. B-1). Assume the total current I behind the projectile is constant, then the position X of the armature (assumed to have zero thickness) is given by,

$$X = \frac{1}{2} \iint a \, dt^2 = \frac{1}{2} a t^2 \qquad (B-4)$$

where a and m are the acceleration and mass of the projectile, respectively. The skin depth, $\delta(x)$, at point, x, along each rail is given by,

$$\delta(x) = \left(\frac{2\rho \Delta t(x)}{\pi \mu} \right)^{1/2} \qquad (B-5)$$

where Δt is the time since the time $t(x)$ of the passage of the armature at point x.

From Eq. (B-4),

$$x = \frac{1}{2} a t(x)^2 \ , \qquad (B-6)$$

we have

$$\Delta t = t - t(x) = \left(\frac{2}{a} \right)^{1/2} \left(x^{1/2} - x^{1/2} \right) \ . \qquad (B-7)$$

Hence,

$$\delta(x) = \left[\frac{2\rho}{\pi\mu}\left(\frac{2}{a}\right)^{1/2}\left(X^{1/2} - x^{1/2}\right)\right]^{1/2} \tag{B-8}$$

A short element dx of resistance R(x) at the point x is,

$$R(x) = \frac{\rho\,dx}{p\delta(x)} \quad, \tag{B-9}$$

where p is the width of the rails. The total resistance R of each rail is then

$$R = \int_0^X R(x)\,dx = \int_0^X \frac{\rho\,dx}{p\delta(x)} \quad. \tag{B-10}$$

Substituting B-8 into B-10 we get,

$$R = \int_0^X \frac{\rho\,dx}{p\left[\frac{2\rho}{\pi\mu}\left(\frac{2}{a}\right)^{1/2}\left(X^{1/2} - x^{1/2}\right)\right]^{1/2}} \tag{B-11}$$

$$= \frac{1}{p}\left(\frac{\pi\mu\rho}{2}\right)^{1/2}\left(\frac{a}{2}\right)^{1/4}\left(\frac{8}{3}X^{3/4}\right) \quad. \tag{B-12}$$

The average resistance gradient, R_1, is

$$R_1 = \frac{R}{X} = \frac{8}{3p}\left(\frac{\pi\mu\rho}{2}\right)^{1/2}\left(\frac{a}{2}\right)^{1/4}X^{-1/4} \tag{B-13}$$

$$= \frac{8}{3p}\left(\frac{\pi\mu\rho}{2t}\right)^{1/2} \quad. \tag{B-14}$$

(Note that B-14 compared to the uniform diffusion case of B-3 indicates a resistance increase by a factor of 8/3.)

The above result is for constant current resulting in constant acceleration. In the case of nonconstant current, the rate of change of current is usually slow resembling a quasi-constant current. Furthermore, the majority of the resistance is in the region close behind the projectile because the current has had less time to diffuse into the rails in that region. This further lessens the effect of time variation of current on the resistance. Hence, Eq. (B-14) is a reasonable approximation of the resistance for most of the railguns we have modeled.

APPENDIX C. TIME-DEPENDENT MFCG INDUCTANCE GRADIENT

The intense currents in the MFCG railgun system generate intense magnetic fields which together exert strong forces on all the current carriers, (the same forces that accelerate the projectile). These forces drive the inertially but not rigidly confined MFCG conductors apart. The increased spacing of the conductors leads to an increase in inductance gradient which influences the overall system operation.

The force F per unit length z driving the MFCG conductors apart is,[7]

$$\frac{F}{z} = \frac{\mu_0}{2\pi}\left(\frac{1}{P_F}\right)^2 \left[2\ P_F\ \tan^{-1}\!\left(\frac{P_F}{w_F}\right) - w_F \ln\!\left(\frac{w_F^2 + P_F^2}{w_F^2}\right)\right] \qquad (C-1)$$

where W_F and P_F are the separation and width of the MFCG conductors. The inductance gradient, L_{1F}, of the MFCG conductor pair can be approximated by

$$L_{1F} \equiv L/z = 0.794 \left[\tan^{-1}\!\left(w_F/P_F\right)\right]^{1.021} \qquad . \qquad (C-2)$$

The form of C-1 is taken from Ref. 8 and normalized to the measured inductance of the MFCG. It is a close fit for w_F/P_F ratios from its initial value of 1 to more than its expanded value of about 2.

The complete time- and current-dependent performance of the MFCG is modeled with Eqs. (C-1) and (C-2) and the appropriate derivatives.

TABLE 1. Summary of results for the LLNL/LANSL Railgun Experiments.[5]

	Experiment							
	1A	1C	2A	2B	2C	2D	2E	50-1
Accelerator length (m)	0.9	0.9	1.8	1.8	1.8	1.8	1.8	.27
Accelerator bore (mm)	12.5	12.7	12.7	12.7	12.7	12.7	12.7	50
Projectile mass (g)	2.9	3.1	3.1	3.1	3.1	3.1	3.1	165
Bank capacitance (mF)	1.5	1.5	3.0	3.0	3.0	3.0	3.0	3.0
Charge voltage (kV)	9.5	16.2	11.5	16.1	16.2	16.1	16.1	16.0
Initial energy (kJ)	68	197	198	389	394	389	389	384
Initial current (kA)	285	~450	440	~640	640	625	625	630
Peak current (kA)	575	~800	~800	~970	965	1200	~1250	1950
Launch velocity (km/s)	2.8	5.6	5.4	~9.9	~9.9	~10.1	~10.1	0.35

FIGURE CAPTIONS

FIG. 1. Schematic of railgun showing the current path I, the magnetic flux lines B, and the resultant force F that drives the projectile. Initially there is a thin metallic fuse in back of the projectile that completes the circuit; this vaporizes almost immediately forming a plasma that continues to carry current and accelerate the projectile in the direction Z.

FIG. 2. Side view of a magnet flux compression generator. When the detonator ignites the high explosive, the top conductor is driven down to short the bottom conductor. The explosive then causes the short to propagate in the z direction, compressing the enclosed flux.

FIG. 3. Electrical equivalent circuit of Railgun. $R(x,t,I)$ and $L(x)$ are the lumped equivalents of the rail resistance and inductance which change as the projectile moves down the railgun. The fuse is first vaporized to initiate the plasma arc and start the projectile acceleration. V_{Arc} is the plasma arc voltage drop (typically 50-300 V).

FIG. 4. MFCG equivalent circuit. The closure of S_1 initiates the discharge of the capacitor bank into the MFCG-Railgun system. The closure of S_2 corresponds to the beginning of the MFCG implosion and R_F and L_F are the lumped equivalents of the MFCG resistance and inductance which decrease with time.

FIG. 5. Complete equivalent circuit of MFCG-powered Railgun.

FIG. 6. Computed and measured magnetic flux compression generator current into a low-inductance short circuit shown as a function of time. The 1.5 mf capacitor bank was initially charged to 10 kV.

FIG. 7a. Computed and measured current for experiment 1A.

FIG. 7b. Computed projectile velocity for experiment 1A.

FIG. 7c. Computed projectile position as a function of time for experiment 1A.

FIG. 8a. Computed and measured current pulse into 50-mm bore railgun vs time for experiment 50-1.

FIG. 8b. Computed projectile position as a function of time for 50-mm bore railgun with 165-g projectile.

FIG. 8c. Computed projectile velocity vs. projectile position for experiment 50-1.

FIG. 9a. Computed and measured current for experiment 2C.

FIG. 9b. Computed projectile position as a function of time for experiment 2C.

FIG. 9c. Computed projectile velocity vs projectile position for experiment 2C.

FIG. A-1. Normalized current diffusion vs depth in copper for a current concentration of 0.5 MA/cm.

FIG. A-2. Temperature vs depth in copper for . current concentration of 0.5 MA/cm.

FIG. A-3. Resistivity vs depth in copper for a current concentration of 0.5 MA/cm.

FIG. A-4. Equivalent resistivity of copper vs current concentration.

FIG. B-1. Representation of current difusion into a rail behind an accelerating projectile. The current diffusion is shown in terms of the equivalent skin depth.

Projectile

Moveable armature

Rigid conducting rails

B

F

B

I

Current source

Z

Deadrick - Fig. 1

Point A
Steel bar
Detonator
Top conductor
Switch
Explosive
Output terminals
z
To Railgun
Capacitor bank (600 kJ, 20 kV)
z_0
Bottom conductor
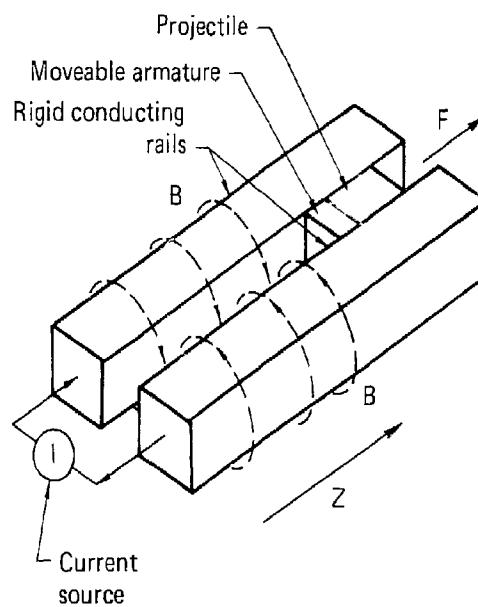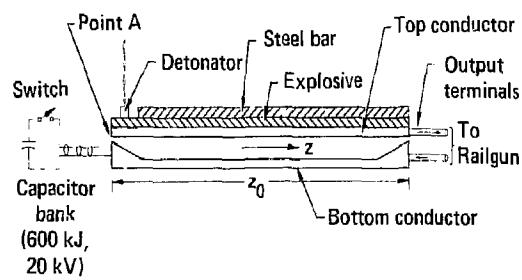
Deadrick - Fig. 2

Deadrick - Fig. 4

Capacitor bank   MFCG   Railgun
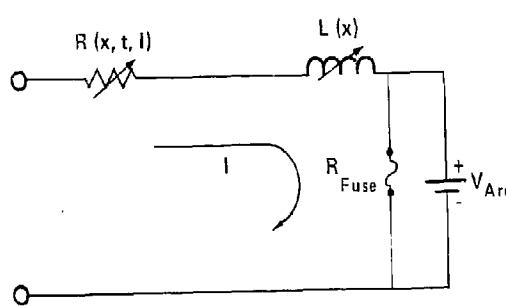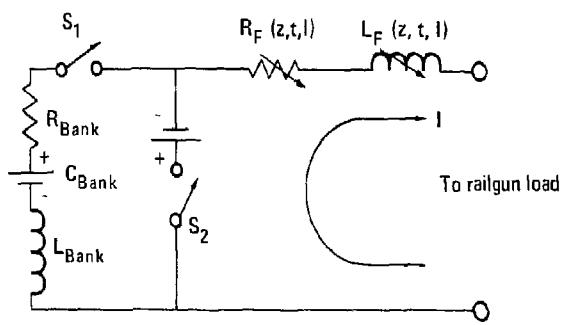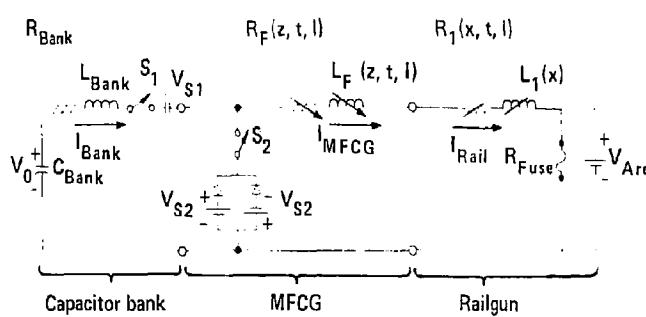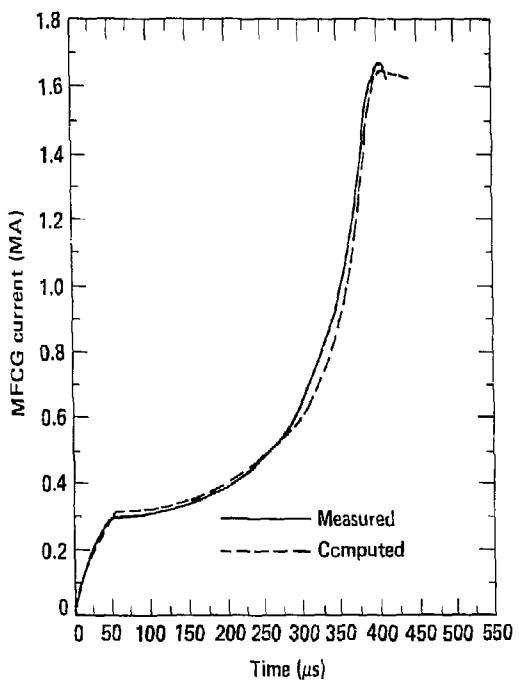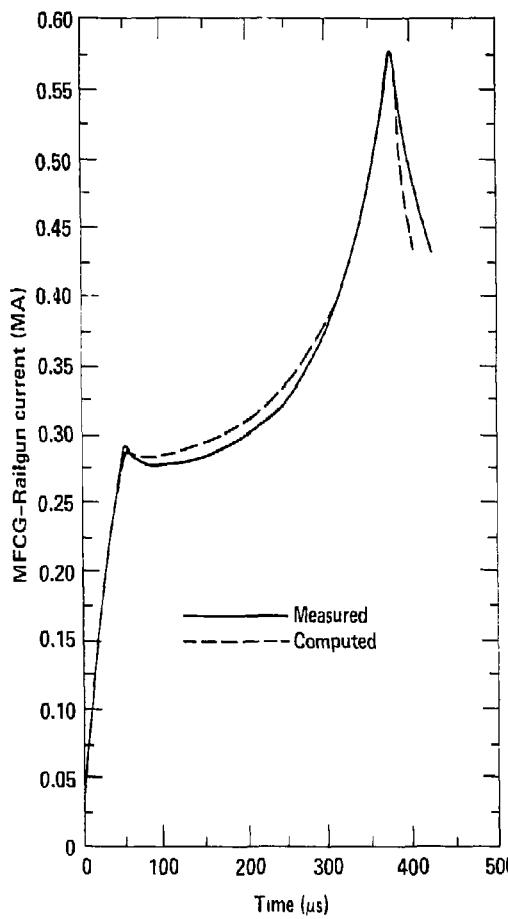
Deadrick - Fig. 6

Deadrick – Fig. 7a

Deadrick – Fig. 7b

Plot of Projectile position (m) versus Time (μs), with an X-ray shadowgraph data point marked near 770 μs at approximately 1.35 m.
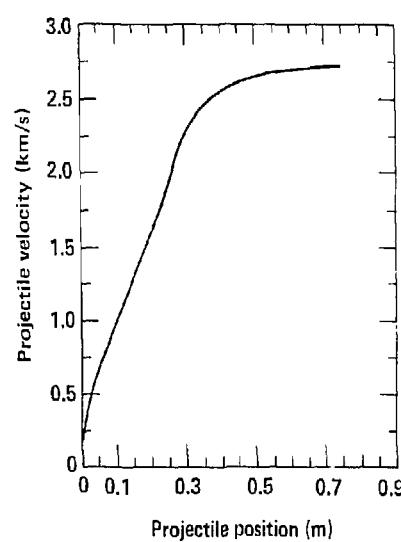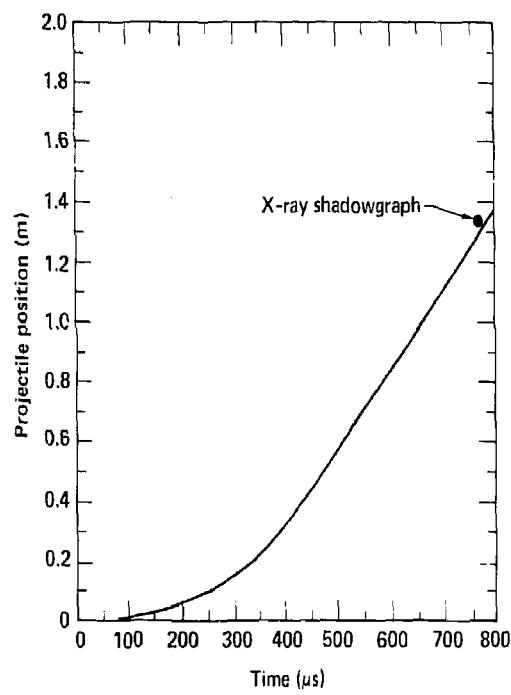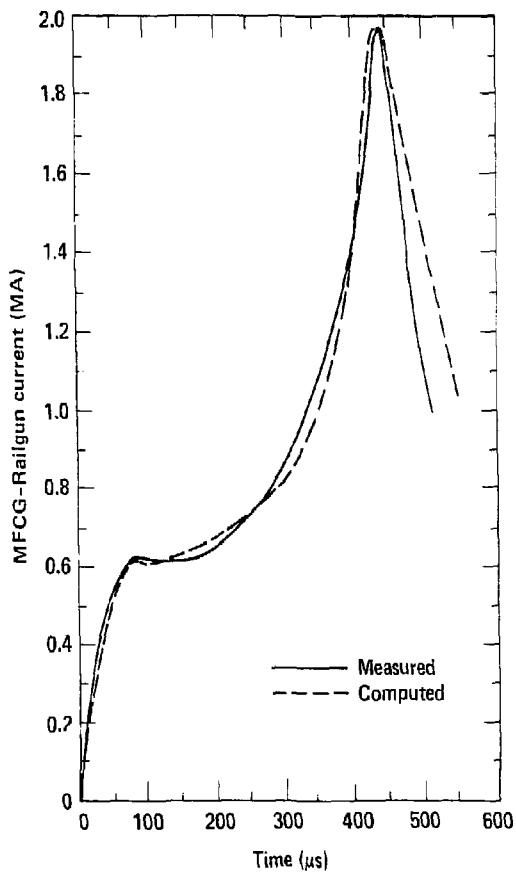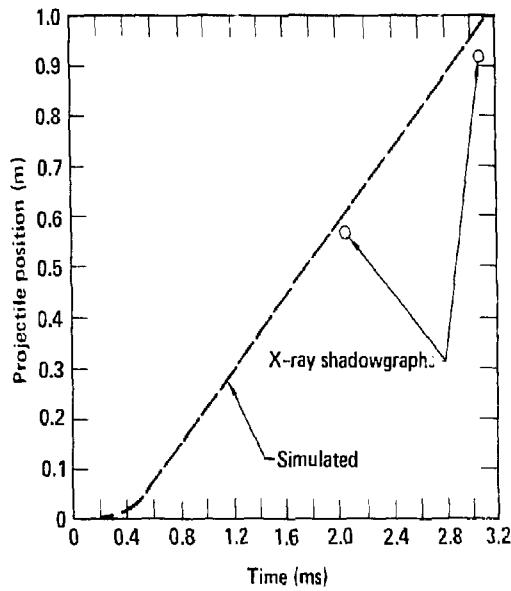
Deadrick - Fig. 8a

Deadrick - Fig. 8b
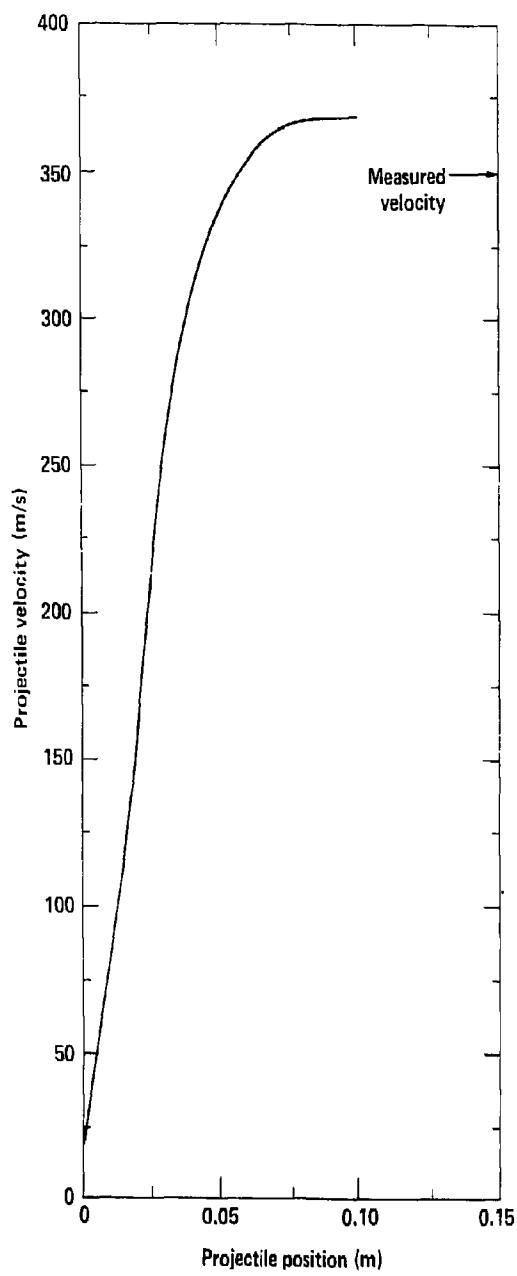
Deadrick - Fig. 8c
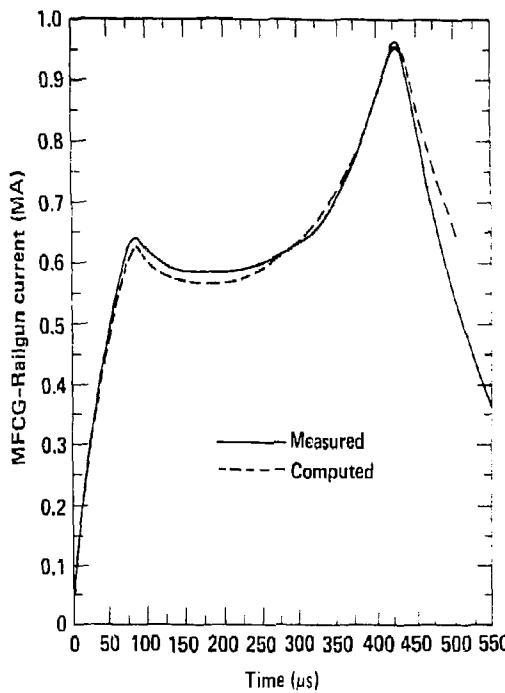
Deadrick - Fig. 9a

Deadrick - Fig. 9b

Velocity (km/s) vs Projectile position (m)

Deadrick - Fig. 9c

Normalized current concentration (MA/cm)

Depth (mm)

2   4   6   8   10 μs

Deadrick – Fig. A–1.

Depth (mm)
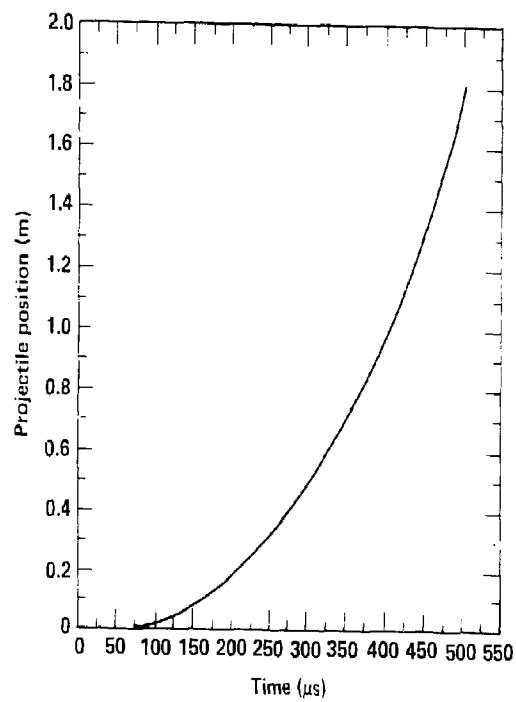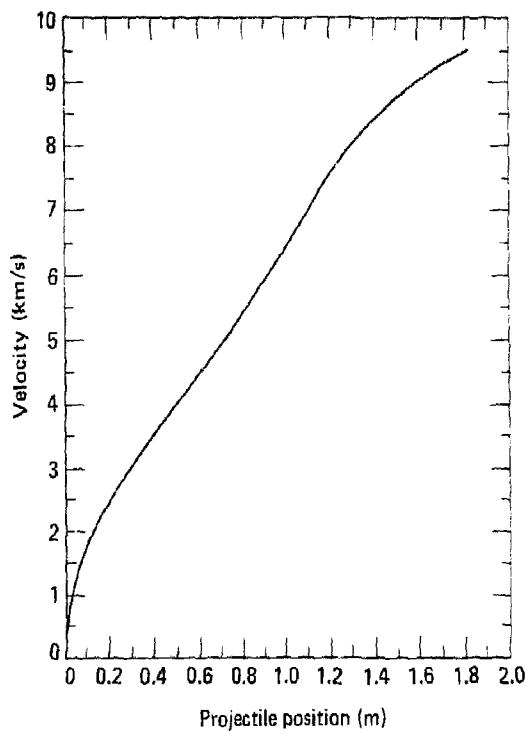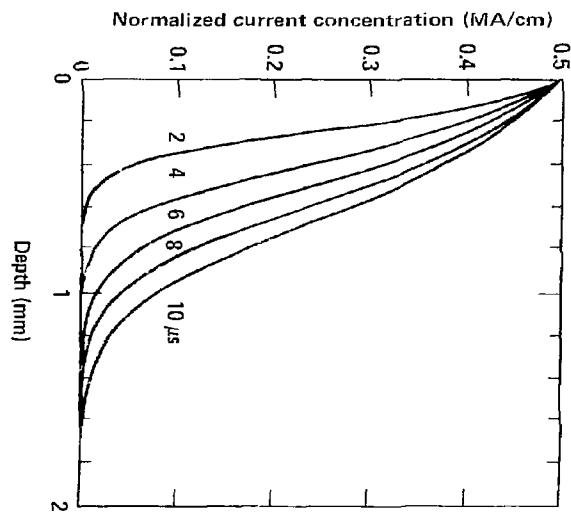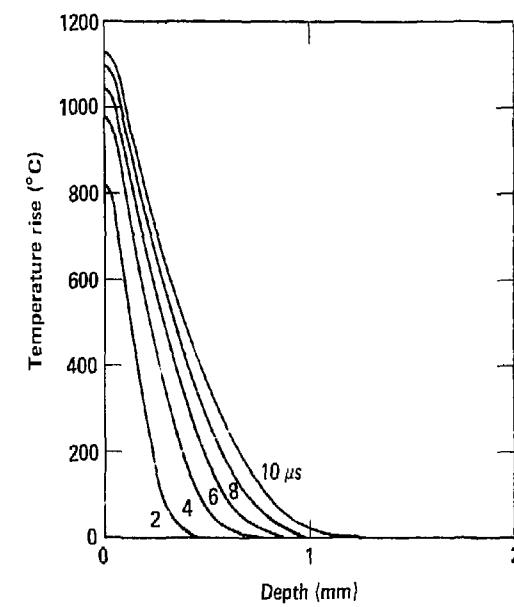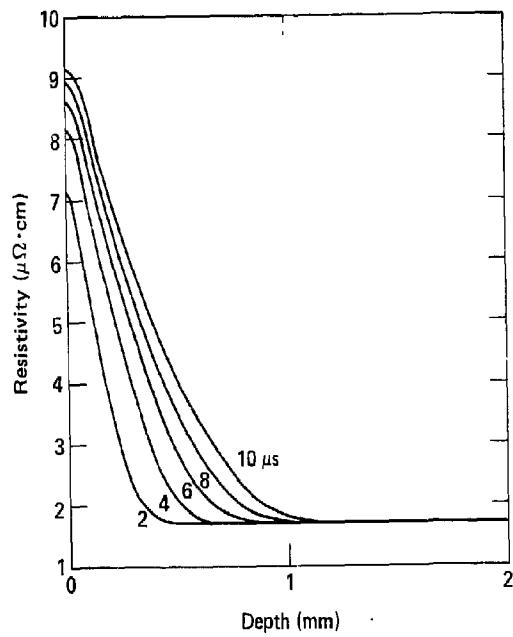
Deadrick – Fig. A-3.

Deadrick – Fig. A-4.

Direction of motion

Projectile

dx

δ(x)

x

Rail

X